PCCP

Accepted Manuscript

This is an *Accepted Manuscript*, which has been through the Royal Society of Chemistry peer review process and has been accepted for publication.

Accepted Manuscripts are published online shortly after acceptance, before technical editing, formatting and proof reading. Using this free service, authors can make their results available to the community, in citable form, before we publish the edited article. We will replace this *Accepted Manuscript* with the edited and formatted *Advance Article* as soon as it is available.

You can find more information about *Accepted Manuscripts* in the Information for Authors.

Please note that technical editing may introduce minor changes to the text and/or graphics, which may alter content. The journal's standard Terms & Conditions and the Ethical guidelines still apply. In no event shall the Royal Society of Chemistry be held responsible for any errors or omissions in this *Accepted Manuscript* or any consequences arising from the use of any information it contains.

ROYAL SOCIETY OF CHEMISTRY

www.rsc.org/pccp

Physical Chemistry Chemical Physics Accepted Manuscript

Computational Studies of Electrochemical CO_2 Reduction on Subnanometer Transition Metal Clusters

*Cong Liu, Haiying He, Peter Zapol and Larry A. Curtiss**

Materials Science Division, Argonne National Laboratory, 9700 S Cass Ave. Lemont IL 60439 USA

*(L.A.C.) Email: curtiss@anl.gov Tel: +1(630)252-7380 Fax: +1(630)252-9555

Abstract

Computational studies of electrochemical reduction of CO_2 to CO, HCOOH and CH_4 were carried out using tetra-atomic transition metal clusters (Fe_4, Co_4, Ni_4, Cu_4 and Pt_4) at the B3LYP level of theory. Novel catalytic properties were discovered for these subnanometer clusters, suggesting that they may be good candidate materials for CO_2 reduction. The calculated overpotentials of producing CH_4 are in the order: $Co_4 < Fe_4 < Ni_4 < Cu_4 < Pt_4$ with both Co_4 and Fe_4 having overpotentials less than 1 V. Investigation of the effects of supports found that a Cu_4 cluster on a graphene defect site has a limiting potential for producing CH_4 comparable to that of a Cu (111) surface. However, due to the strong electronic interaction with the Cu_4 cluster, the defective graphene support has the advantage of significantly increasing the limiting potentials for the reactions competing with CH_4, such as the hydrogen evolution reaction (HER), and CO production.

Introduction

The conversion of CO_2 to fuels is of use of renewables in carbon-neutral technologies and for developing approaches to mitigate global warming. High thermodynamic stability of the CO_2 molecule requires substantial input of energy for its reduction and conversion. Studies of catalytic reduction of CO_2 to useful chemicals, such as CO, HCOOH, CH_3OH, CH_4 and longer-chain hydrocarbons, have been focused on three major approaches: chemical[1-4], electrochemical[2, 5-10] and photochemical reductions[2, 11, 12]. During the last three decades, electrochemical reduction of CO_2 has gained increasing interest from both academia and industry. CO_2 dissolved in liquids can be electrocatalytically converted into various hydrocarbons and oxygenates directly at the

surface of solid electrodes[2, 7-9, 11]. Moreover, homogeneous catalysts can be incorporated with the solid electrodes to facilitate the electron transfer during CO_2 reduction[2, 13]. This approach holds promise in the utilization of renewable electricity (e.g., from solar and wind power). Compared to catalytic chemical reduction of CO_2, electrochemical reactions provide three advantages in industrial processes.[8] First, the surface free energy of the catalyst is easily altered through the electrode potential, which allows precise control of the reaction rate and product selectivity. Secondly, the achievable efficiency of electrochemical devices is significantly higher than the traditional chemical reactors, because the former are not limited by thermochemical cycles. Finally, because of the non-direct reaction between precursors through redox processes on two separate catalysts, catalysts can be tailored for each redox process independently. In addition, electrochemical reduction of CO_2 is, to some extent, a more straightforward technology compared to photocatalysis, without having to consider the photon efficiency of the catalytic materials[2].

Electrochemical reduction of CO_2 to fuels has been investigated both experimentally and computationally using various transition metal electrodes[7, 14-17]. Most of the previous studies have been focused on single crystal electrodes. Hori et al. discovered experimentally that CO_2 is reduced to CH_4, C_2H_4 and alcohols at Cu electrodes, with overpotentials on the order of 1 V[7, 15]. More importantly, the surface orientation of Cu crystal plays a significant role in the selectivity of the products. For instance, CH_4 formation is favored at Cu(111), while C_2H_4 is more likely to form at Cu(100)[18]. The reaction mechanisms of the formation of CH_4 and longer chain hydrocarbons on Cu electrodes were studied computationally by the Norskov group[17] and the Koper group[16, 19]. In addition, Pt[20], Ir[21] and Rh[22] single crystals were also found to reduce CO_2 electrochemically. More recent studies of electrochemical reduction of CO_2, on the other hand, have been carried out using a number of novel metal materials, such as supported metal nanoparticles[6, 9, 23-26], metal alloys[27] and metal or metal oxide overlayers[28, 29]. In particular, Centi et al.[9] first utilized Pt nanoparticles on carbon based electrodes (e.g., carbon black (Vulcan XC-72) and/or carbon cloth) to convert CO_2 electrochemically to long carbon-chains (>C5) at room temperature and atmospheric pressure. Gangeri et al.[6] later studied conversion of CO_2 to oxygenates (e.g., isopropanol) using Pt and Fe nanoparticles supported on carbon nanotube (CNT) electrodes, showing that Fe particles have a higher activity than Pt particles, although they also deactivate faster. Furthermore, a recent experimental study by Reske et al.[28] on CO_2

Physical Chemistry Chemical Physics Accepted Manuscript

reduction on Cu overlayers on Pt electrode suggested that the catalyst's activity is improved with increasing copper layer thickness, and the formation of methane decreases much faster than that of ethylene with decreasing Cu layer thickness. All these studies suggest that the reactivity and product selectivity of the catalysts for CO_2 electrochemical reduction are essentially controlled by two major components: the geometric effect (e.g., surface structure and particle size) and the electronic effect (e.g., type of metal).

Recently, size-selected subnanometer transition metal clusters have gained great attention in catalysis[30-41], due to their unique electronic and catalytic properties, which deviate from extended metal surfaces and larger nanoparticles[40]. Typically, for very small clusters (diameters below around 2 nm), quantum effects become noticeable, referred to as the "catalytic finite-size effect".[42] Vajda et al. have successfully synthesized subnanometer metal and metal oxide clusters with very narrow size distributions on thin film support materials (e.g. alumina)[31, 33-35, 37, 40, 43]. These materials have shown great potential in the catalysis of electrochemical reactions. For instance, the electrocatalysis of water oxidation was studied using Pd_4, Pd_6 and Pd_{17} clusters on a ultrananocrystalline diamond Si-coated electrode[35], indicating that these clusters have stable electrochemical potentials over several cycles. The catalyst system showed no evidence of evolution or dissolution of either the electrode material or the clusters[35]. Also, studies by Proch et al. on electrocatalysis of carbon oxidation using Pt_n ($n \leq 11$) clusters indicated that Pt clusters are much more reactive than Pt nanoparticles under similar conditions[44]. Moreover, electrochemical reduction of CO_2 using Au_{25} clusters has been investigated by Kauffman et al.[45], showing that Au_{25} clusters represent a remarkable improvement over larger Au nanoparticles and bulk Au. Despite the increasing reports on electrocatalysis of CO_2 and applications of size-selected subnanometer clusters, no detailed mechanistic studies have been carried out on electrochemical reduction of CO_2 using size-selected subnanometer transition metal clusters.

Previously, we have studied reaction mechanisms of homogeneous and heterogeneous catalysis of CO_2 reduction using surfaces and complexes of 3d transition metal catalysts[46-49], as well as photocatalytic reduction of CO_2 on TiO_2 surfaces[50-53]. In this contribution, computational studies of electrochemical reduction of CO_2 using tetra-atomic metal clusters are presented. Initially, chemisorption and electrochemical adsorption of CO_2 on ten metal clusters (Fe_4, Co_4, Ni_4, Cu_4, Ir_4, Pd_4, Ag_4, Rh_4, Pt_4 and Au_4) was investigated. Then, Fe_4, Co_4, Ni_4, Cu_4 and Pt_4 clusters were selected to study the reaction mechanisms of electrochemical reduction of CO_2 to

Physical Chemistry Chemical Physics Accepted Manuscript

CO, HCOOH and CH_4, as well as the hydrogen evolution reaction. Possible chemical and electrochemical reactions were taken into account, and the most favorable reaction pathway was identified. The over-potentials for producing CH_4 were derived using volcano plots. Lastly, the reaction thermodynamics of the isolated Cu_4 cluster was compared with that of the Cu_4 cluster deposited on a graphene sheet and a defective graphene sheet. We also make a comparison to previous results using Cu nanoparticles and surfaces and discuss the potential for use of size selected clusters for CO_2 reduction.

Computational Details

Geometry optimizations and free energy calculations of all the unsupported clusters were carried out using the density functional (DFT) method B3LYP[54, 55] with the Gaussian09 program package[56]. The structures of the tetra-atomic clusters used in this work are the lowest energy structures calculated using B3LYP. The B3LYP density functional predictions of the ground-state geometries and spin states of the tetra-atomic clusters[40] considered in this work are comparable to previous studies of these clusters (See Section S1, Supporting Information). Single-point calculations of binding energies of CO_2 to all ten clusters were also carried out using the M06[57] and PBE0[58-60] methods, with B3LYP thermo corrections. CCSD(T)[61] single point energies were also calculated for Cu, Ag and Au clusters. The B3LYP binding energies are in reasonable agreement with these other methods in most cases (For a detailed analysis, see Section S1, Supporting Information). The 6-31G* basis set was used for all the main group elements (C, O, H). An improved 6-31G* basis set proposed by Mitin et al.[62], m6-31G*, was utilized for all the 3d metals, and the LANL2DZ basis set[63-65] was used for all the 4d and 5d metals. The partial charges of adsorbed CO_2 on the clusters were calculated using natural bond orbital (NBO) analysis[66-71]. The transition states of the C-O bond-breaking reactions were calculated using QST3 method and were confirmed using intrinsic reaction coordinate (IRC) calculations.

A reaction network containing 38 intermediates for possible electrochemical and chemical reactions was analyzed to identify the most favorable electrochemical reaction pathway for each considered cluster system (see Section S2 in Supporting Information). Multiple conformations and spin states for all the metal clusters and intermediates were considered to locate lowest

Physical Chemistry Chemical Physics Accepted Manuscript

energy geometries and multiplicities. (For the ground-state multiplicities and relative energies of the species in the pathways see Sections S1 and S3, Supporting Information).

Each electrochemical reaction step considered in the present work involves a proton-electron pair transfer from solution to an adsorbed species on the cluster. The free energy change of each proton transfer reaction step was calculated using the computational hydrogen electrode (CHE) method suggested by Norskov et al.[17, 72, 73]. The reaction free energy of each elementary reaction can be calculated using Equation 1:

$$\Delta G_{ele} = \mu[\text{Product}] - \mu[\text{Reactant}] - 0.5\mu[H_{2(g)}] + eU \quad (1)$$

where ΔG_{ele} represents the free energy change of the elementary step, μ is chemical potential and U is applied electrical potential. When U = 0V, ΔG_{ele} equals to the limiting potential (U_L) of elementary hydrogenation reaction. Previous calculations have been carried out for the electrochemical proton transfer barriers of the reduction of O_2 to OOH on Pt[74] and of the reduction of OH to H_2O on Pt[75], showing that these barriers are from 0.15eV to 0.25eV at zero applied voltage, and diminish with higher applied voltages. Such barriers are easy to overcome at room temperature[17]. Therefore, it is assumed in the present work that the reaction free energy of an electrochemical proton transfer reaction is a good measure of the favorability of the reaction. However, such an assumption does not apply to chemical reactions such as C-O bond breaking of an adsorbate on the cluster. Thus, the barriers of these reactions were calculated. The CHE method circumvents the explicit quantum mechanical calculations for solvated protons and all the solvent effect on geometries and free energies were neglected. All the Gibbs free energies were calculated in gas phase at 25°C, in which all the gaseous molecules (CO_2, CO, H_2 and CH_4) and all the metal cluster-containing systems were calculated under the standard pressure, 101325Pa, while the liquid phase molecules (H_2O, HCOOH and CH_3OH) were calculated under their corresponding vapor fugacity, which comes from their vapor-liquid equilibrium with water corresponding to a liquid mole fraction of 0.01[17]. (See details are in Section S1, Supporting Information). Selected Cu_4 reactions were also calculated at 18.5°C for comparison.

Graphene supported Cu_4 systems were calculated with the Vienna Ab initio Simulation Package [76-79] (VASP, version 5.3.2), using the PBE functional[58] with a plane wave basis set. A graphene supercell with 72 carbon atoms was built with a 2.46Å lattice constant and 15Å of vacuum space. A model for a defect site in graphene was made with one carbon vacancy and is referred to as "defective" graphene in this paper. During the simulation the positions of all atoms

Physical Chemistry Chemical Physics Accepted Manuscript

in the systems were allowed to relax, while the shape and size of the supercell was fixed. The energy cutoff was 400 eV, with a 2×2×1 k-point grid and a Fermi-level smearing width of 0.2 eV. Free energies of adsorbates were calculated by treating 3N degrees of freedom of the adsorbate as vibrational. It is assumed that changes in the vibrations of the graphene support were minimal.[17] Vibrational modes were calculated using a normal-mode analysis. Zero-point energies, entropies and heat capacities were calculated from these vibrations to convert the electronic energies into free energies at 18.5°C (for comparison with previous computational studies). Non-adsorbed molecules were calculated using the same techniques, except with a Fermi-level smearing of 0.01 eV (Corrections to the non-adsorbed species see Section S1, Supporting Information).

Results and Discussion

1. *Chemisorption vs. Electrochemical Adsorption of CO_2 on Tetra-atomic Metal Clusters*

We first investigated whether, under electrochemical conditions, chemisorption or electrochemical adsorption of CO_2 is more likely to occur. Equations 2 and 3 are typical representations for the chemisorption and the electrochemical adsorption of CO_2 on a heterogeneous catalyst, respectively.

$$CO_2 + * \rightarrow CO_2* \qquad (2)$$

$$CO_2 + H^+ + e^- + * \rightarrow COOH* \qquad (3)$$

The chemisorption of CO_2 often involves a charge transfer from the catalyst to CO_2[47, 49], while the electrochemical adsorption of CO_2 involves a proton-electron pair transferred to CO_2. The former mainly depends on the intrinsic properties of the catalyst, while the latter can be controlled by an applied electric potential. In this section, the thermodynamics of chemisorption and electrochemical adsorption (without applied potential) of CO_2 on tetra-atomic clusters are discussed. Middle to late transition metal clusters, Fe_4, Co_4, Ni_4, Cu_4, Ir_4, Pd_4, Ag_4, Rh_4, Pt_4 and Au_4 were considered.

The structures of the clusters and CO_2-cluster adsorbate complexes, the calculated partial charges on the adsorbed CO_2 and adsorption free energies are shown in Table 1 (For the details of structures and spin-states of all species see Section S2, Supporting Information). In general,

Physical Chemistry Chemical Physics Accepted Manuscript

CO_2 binding to Fe_4, Co_4, Ni_4, Cu_4, Rh_4 and Pt_4 clusters involves a significant reduction of the O-C-O angle, as well as a charge transfer from the cluster to CO_2, while for Pd_4, Ag_4, Ir_4 and Au_4, CO_2 maintains a nearly linear structure and little charge transfer occurs. The calculated adsorption free energies of CO_2 indicate that only Fe_4, Co_4 and Ni_4 clusters have favorable interactions with CO_2, while the other clusters showed positive adsorption free energies (Table 1). A positive adsorption free energy generally suggests that adsorption on the cluster is unlikely to happen spontaneously. Therefore, chemisorption of CO_2 on Fe_4, Co_4 and Ni_4 clusters is much more favorable than that on the other metal clusters.

In comparison, the electrochemical adsorption of CO_2 on all clusters involves a ($H^+ + e^-$) transfer resulting in a significant reduction in the O-C-O angle (Table 1). For Fe_4, Co_4, Ni_4, Cu_4, Rh_4, Ag_4 and Ir_4, the COOH adsorbate binds to the cluster through both C and O atoms, while for Pd_4, Pt_4, and Au_4 only the C atom is bound to the cluster. The calculated reaction free energies show that the electrochemical adsorption of CO_2 favors Co_4 and Ni_4 clusters with no applied potential, while all the other clusters require an applied potential for the reaction to occur. It is notable that Ag and Au clusters gave high reaction free energies (1.40 and 1.43 eV, respectively), which lead to high over-potentials of the electrochemical reaction, and are not catalytically favorable. It is also interesting that, for Fe_4, Co_4 and Ni_4 clusters, the adsorption of CO_2 (Equation 2) is thermodynamically more competitive (with more negative reaction free energies) than the electrochemical adsorption (Equation 3). Therefore, when considering these three clusters for the electrochemical reduction of CO_2 to fuels (e.g., CH_4), the reaction pathways initiated by both chemisorption and electrochemical adsorption of CO_2 need to be taken into account. In this work, Fe_4, Co_4, Ni_4, Cu_4 and Pt_4 clusters were selected to study the reaction mechanisms of electrochemical reduction of CO_2 to CH_4, CH_3OH, CO and HCOOH. Larger nanoparticles of these five metals have been reported previously[6, 80-82] in the applications of electrocatalysis, and showed reasonable stability under acidic conditions.

2. *Electrochemical Reduction of CO_2 to CH_4*

The CHE model was applied to the electroreduction of CO_2 by investigating a reaction network including possible electrochemical and chemical bond cleavage reactions associated with reduction of CO_2 to the major products CO, HCOOH and CH_4 (for the reaction network see

Physical Chemistry Chemical Physics Accepted Manuscript

Section S2, Supporting Information). In general, the reaction pathways in the network may be initiated by three reactions, shown in Equation 2, 3 and 4, respectively.

$$CO_2 + H^+ + e^- + * \rightarrow OCHO* \qquad (4)$$

The reaction free energies of all elementary steps in the reaction network were calculated (Section S2, Supporting Information), and the barriers of the possible chemical bond cleavage reactions were taken into account (Section 2.1). Thermodynamically most favorable pathways and major side reactions were identified based on the reaction network for all five clusters (Section 2.1 and 2.2), and the activity descriptors for the formation of CH_4 were analyzed (Section 2.3).

2.1 C-O Bond Cleavage

In an electrochemical reaction, a C-O bond cleavage is often a multi-step reaction, which involves the hydrogenation of the oxygen atom and the release of water. A C-O bond can also be cleaved directly by the catalyst. Our previous studies[49] have shown that Fe, Co and Ni fcc (100) surfaces chemically break the C-O bond of CO_2 spontaneously with low barriers. Thus, in this study, possible C-O bond breaking reactions were considered to study the catalytic properties of the metal clusters. As mentioned earlier, catalytic bond breaking reactions are different from the electrochemical proton transfer reactions, and the barriers of the former cannot be ignored. Therefore, both reaction free energies and barriers of three possible C-O bond breaking reactions were studied for the five metal clusters (Fe_4, Co_4, Ni_4, Cu_4 and Pt_4). Equations 5, 6 and 7 represent the C-O cleavage of CO_2*, CHO* and OCHO*, respectively.

$$CO_2* \rightarrow CO* + O* \qquad (5)$$

$$CHO* \rightarrow CH* + O* \qquad (6)$$

$$OCHO* \rightarrow CHO* + O* \qquad (7)$$

The chemisorption of CO_2 (Equation 2) is followed by the C-O cleavage of CO_2* (Equation 5). Equation 6 may occur after CHO* is formed. Equation 7 is the reaction following Equation 4. These reactions result in a carbon-oxygen bond breaking.

Physical Chemistry Chemical Physics Accepted Manuscript

The Brønsted–Evans–Polanyi (BEP) relations of the reaction free energies and barriers were developed for the three C-O cleavage reactions shown in Figure 1. To begin with, as shown in Figure 1(a), reaction A is exergonic for Fe_4, Co_4 and Ni_4 clusters, but endergonic for Cu_4 and Pt_4 clusters. In other words, the direct C-O cleavage of CO_2* is spontaneous on Fe_4, Co_4 and Ni_4 clusters. In addition, these three metal clusters show low barriers (<1.00 eV, Figure 1(a)), which allow the reactions to occur at room temperature, while both Cu_4 and Pt_4 systems gave barriers higher than 1.50 eV. For the C-O cleavage of CHO*, on the other hand, only Fe_4 and Co_4 clusters showed negative reaction free energies, while the reaction is endergonic for the other clusters (Figure 1(b)). Moreover, all the clusters except for Fe_4 showed extremely high barriers (>2.00 eV). This indicates that the C-O cleavage of CHO* is only likely to occur on Fe_4 cluster at room temperature. Finally, the C-O cleavage of OCHO*, as shown in Figure 1(c), is endergonic and shows high barriers (>1.50 eV) for all five metal clusters. In summary, the C-O cleavage of CO_2* is likely to happen directly through Fe_4, Co_4 and Ni_4 clusters, as well as the C-O cleavage of CHO* on Fe_4 cluster. These exergonic chemical reactions with low barriers can compete with the electrochemical reactions, and therefore shall be included in the mechanism studies of the Fe_4, Co_4 and Ni_4 systems.

2.2 Reaction Mechanisms of Electrochemical Reduction of CO_2 to CH_4

2.2.1 Fe_4, Co_4 and Ni_4 Clusters

Figure 2 shows the reaction coordinates of CH_4 formation on a Fe_4 cluster. The lowest energy electrochemical pathway (pathway 1) was identified, shown in black, Figure 2(a). The reaction pathway initiated by CO_2 chemisorption was also considered (pathway 2, red, Figure 2(a)). In the lowest energy electrochemical pathway (pathway 1), CO_2 and a ($H^+ + e^-$) pair first forms COOH adsorbed on the cluster (state **2**, Figure 2), then the hydroxyl group undergoes further hydrogenation and dissociates as an H_2O molecule, and the remaining carbon and oxygen forms CO* (state **3**). The CO* further goes through four degrees of hydrogenation to form CHO* (**4**), CH_2O* (**5**), and then CH_3O* (**6**). The CH_3O* is then hydrogenated on the carbon atom, leading to the production of CH_4. The formation of CH_3OH was found to be less thermodynamically favorable, agreed with previous studies[17]. The remaining adsorbed oxygen (O*, **7**) is then hydrogenated to form OH* (**8**) and eventually dissociates as H_2O. In this reaction path, each elementary step is an electrochemical reaction and requires transfer of one ($H^+ + e^-$) pair.

Physical Chemistry Chemical Physics Accepted Manuscript

According to the CHE model, the rate determining step is the last step, the ($H^+ + e^-$) pair transfer to OH*, which is endergonic by 0.72 eV (Figure 2(a)). This requires a potential of -0.72 V to remove adsorbed OH from Fe_4 cluster.

On the other hand, according to the discussions in the previous Sections, the Fe_4 cluster binds CO_2 and breaks the adsorbed C-O bond spontaneously with a low barrier of 0.63 eV. This suggests that a reaction pathway initiated by the CO_2 chemisorption may also exist (pathway 2, red, Figure 2(a)). In this pathway, CO_2 first chemically binds the cluster and forms CO_2* (**2b**), which goes through a C-O cleavage transition state (**3b**) to form a CO and O co-adsorbed complex (CO* + O*) (**4b**). In the following the adsorbed CO of (CO* + O*) goes through a similar reaction path, with the pathway 1 (black, Figure 2(a)), to produce CH_4. From (CO* + O*) (**4b**) to (CH_3O* + O*) (**7b**), the adsorbed oxygen is thermodynamically stable and likely to stay on the cluster, instead of being hydrogenated. The release of CH_4 leads to two oxygen atoms adsorbed on the cluster 2(O*) (**9b**), in which both oxygens are hydrogenated one after another to form (OH* + O*) (**9b**) and 2(OH*) (**10b**). In the end, the two OH adsorbates are reduced and leave as two H_2O molecules. In this pathway, the first two steps, CO_2 chemisorption and C-O cleavage, are chemical reactions that are not affected by the electrochemical environment, while the other elementary steps are electrochemical reactions. The rate determining step of this pathway is the hydrogenation of one of the two OH's of 2(OH*) (from **10b** → **8**). This step is endergonic and requires a potential of -1.17 V to become exergonic. Compared to the ($H^+ + e^-$) pair transfer to a single adsorbed OH (**8**), it is much more difficult to hydrogenate an adsorbed OH when another OH is co-adsorbed on the cluster. Therefore, the formation of 2(OH*) would be a problem in the electrocatalysis on Fe_4 cluster.

It is worth noting that most of the intermediate states in pathway 2 in Figure 2(a) are energetically lower-lying than the intermediates in pathway 1, relative to the initial reactants (**1**). Moreover, the C-O cleavage transition state lays only 0.07 eV above the initial state (**1**). This indicates that pathway 2 is very likely to occur. However, the CHE model suggests that pathway 1 requires a much smaller potential than pathway 2 for the reaction to occur, and thus is the ideal reaction mechanism. In Figure 2(b), a potential of -0.72 V was applied to the free energy profiles of both pathways. The first two steps of pathway 2 are chemical reactions that are not affected by the electric potential, and the reaction free energies and barriers of these reactions remain the same before and after the external potential is applied. With the applied potential, pathway 1

Physical Chemistry Chemical Physics Accepted Manuscript

generally has lower-lying intermediates than pathway 2; however, pathway 2 could still contribute to the overall reaction and would require a larger potential to remove the OH adsorbates from the catalyst.

Co_4 and Ni_4 clusters showed very similar reaction mechanisms as the Fe_4 clusters. As shown in Figure 3(a) and Figure 4(a), the electrocatalytic (black, pathway 1) and the CO_2 chemisorption initiated (red, pathway 2) pathways of these two clusters gave intermediates similar to the Fe_4 cluster. The rate determining step of pathway 1 is the hydrogenation of the adsorbed OH (OH*, **8**) for both Co_4 and Ni_4, as for the Fe_4 system. Pathway 1 requires a potential of -0.63 V and -1.01 V to proceed for Co_4 and Ni_4, respectively. For both clusters in pathway 2, the intermediate states are much lower lying than those of pathway 1; the rate-determining step is the hydrogenation of one OH of 2(OH*) (**10b** → **8**), the same with the Fe_4 cluster. This pathway requires large potentials of -1.03 V and -1.53 V to proceed for Co_4 and Ni_4 systems, respectively (Figure 3(b) and Figure 4(b). After a potential of -0.63 V was applied to Co_4 and -1.01 V was applied to Ni_4 cluster, pathway 1 showed a more exergonic reaction than pathway 2. And similar to the Fe_4 system, pathway 2 could still proceed at a slower rate and cause the poisoning of the catalyst by engendering 2(OH*).

It is noted that a conformational change of the metal cluster was obtained for the state of Ni_4 system during the reaction. The metal cluster with two adsorbed OH groups changed to a rhombus structure from a tetrahedral structure, while with a single adsorbed OH the cluster keeps a tetrahedral form. This suggests that the strong electronic interaction between the second OH and the cluster leads to the deformation of the close-packed tetrahedral structure.

In summary, Fe_4 and Co_4 clusters are very active for the electrocatalytic reduction of CO_2 to CH_4, with limiting reaction free energies of less than 1 eV, while a Ni_4 cluster showed a larger rate-limiting free energy (1.01 eV). However, spontaneous CO_2 chemisorption and C-O cleavage on these clusters lead to the formation of intermediate states with an extra adsorbed oxygen or a hydroxyl group. These intermediates are lower-lying in the energy profile, and the hydrogenation of the 2(OH*) state is much harder than that of OH*, engendering larger rate-limiting reaction free energies. Although the ideal reaction pathway requires much smaller potentials, larger potentials would be necessary to prevent side reactions and deactivation of the catalyst.

2.2.2 Cu_4 and Pt_4 Clusters

Physical Chemistry Chemical Physics Accepted Manuscript

In the investigations in Section 2.1, Cu_4 and Pt_4 showed very high barriers and endergonic reactions for possible C-O cleavage steps. These reactions are, therefore, unlikely to occur at room temperature for these two clusters. Under the applied potential the only favorable pathway is thus an electrochemical pathway, where each elementary step requires a ($H^+ + e^-$) pair transfer. From the CHE model, the lowest energy pathway was identified for both clusters. The electrocatalysis of CO_2 on Cu_4 and Pt_4 clusters follows a very similar path as the Fe_4, Co_4 and Ni_4 clusters. Shown in Figure 5 and 6, CH_4 formation on both clusters still follows the formation and hydrogenation of CO*, as on the other three metal clusters. However, the hydrogenation of CO* to form CHO* (**3** → **4**), rather than the hydrogenation of OH* for the other clusters (Fe_4, Co_4 and Ni_4), is the rate-determining step of Cu_4 and Pt_4 systems. This is similar to the electrochemical reduction of CO_2 on Cu surfaces from previous studies.[17] The CO* hydrogenation requires a potential of -1.05 V and -1.32V to proceed for Cu_4 and Pt_4, respectively.

2.3 Volcano Plots for the Electrochemical Reduction of CO_2 to CH_4

The five metal clusters (Fe_4, Co_4, Ni_4, Cu_4 and Pt_4) show similar reaction pathways for the electrochemical reduction of CO_2 to CH_4, although the rate-determining step differs. The hydrogenation of *OH is the key step for Fe_4, Co_4 and Ni_4, while the hydrogenation of CO* is the most endergonic step for Cu_4 and Pt_4. Given that similar reaction mechanisms and intermediate species were obtained in the reduction of CO_2 to CH_4 for the five metal clusters, an analysis based on the correlations of the adsorption energies of the intermediate species[73] can be carried out. In the major reaction pathway of all five clusters, the first half of the intermediates (COOH*, CO*, CHO* and CH_2O*) are bound to the cluster through a carbon atom, and the second half (CH_3O*, O* and OH*) interact through an oxygen atom. Previous studies on metal surfaces[73] have suggested that there are strong correlations for the adsorption energies within the carbon-bound and oxygen-bound species. Based on scaling relations and the d-band theory of adsorption, the adsorption free energies of the carbon-bound species of the five metal clusters were correlated to the adsorption free energy of CHO, ΔG_B[CHO], shown in Figure 7(a-c), and the adsorption free energies of the oxygen-bound species were correlated to ΔG_B[OH] shown in Figure 7(d,e).

Physical Chemistry Chemical Physics Accepted Manuscript

The cluster's affinity for the carbon-bound and oxygen-bound species display general trends as a function of metal; for the carbon-bound species, the adsorption free energies are in the order Ni > Co > Fe > Pt > Cu, while the oxygen-bound species follows the order Co > Fe > Ni > Cu > Pt. However, one exception was observed for the CO affinity; the ground state triplet Pt_4(CO) showed an extremely large adsorption free energy, shown to be the outlier in Figure 7(a). It is interesting that the three other carbon-bound species (COOH*, CHO* and CH_2O*) showed strong correlation with each other and were fitted with the other four metal clusters (Figure 7, (b, c)). It is also worth noting that the singlet Pt_4(CO) tends to fit much better with the trend of the four other metal clusters (Figure 7(a)). In order to verify whether B3LYP provided the correct spin state for the ground state of the Pt_4(CO) complex, CCSD(T) single-point calculations were carried out for both singlet and triplet Pt_4(CO), confirming that the triplet is the ground state. This implies that the large CO affinity of Pt_4 cluster could possibly be caused by the higher spin on the Pt_4 cluster. This exception is not the case for bulk Pt surfaces[73], where the ground state of adsorbed CO is a singlet. Moreover, a previous DFT study[83] on CO binding energies of Pt_3 cluster, Pt thin layers and Pt(111) surface found that the Pt_3 cluster exhibits the strongest CO binding among the three materials, and the CO binding energy of the Pt_3 cluster is 1.22 eV higher than that of the bulk Pt surface. Studies also suggested that with the increasing number of layers of the Pt thin films, the CO binding energy decreases rapidly. In the present study of the electrochemical reduction of CO_2 to CH_4, the larger CO affinity of Pt_4 cluster engenders a more stable CO* state relative to the other carbon-bound species shown in Figure 6, and this leads to CO* → CHO* as the rate-limiting step of the Pt pathway and to require a large potential (-1.32 V) to proceed. Although the exact reason for the dramatic CO affinity of Pt clusters is unknown, the catalytic properties of Pt clusters, at this stage, are different from the bulk materials.

Figure 8 shows the elementary limiting potentials (U_L) that scale with ΔG_B[CHO] and ΔG_B[OH]. In Figure 8(a), for example, each line shows the limiting potential (U_L) of an elementary step in the electrochemical pathway. These limiting potentials represent the potentials required for the reaction to proceed, giving a first-order approximation of the electrical potential sufficient to provide a considerable reaction rate[73]. The difference between the most negative U_L and the equilibrium potential (+0.17 V for CO_2 electroreduction to CH_4) represents a theoretical overpotential. In Figure 8(a), two reactions, CO* → CHO* and CHO* → CH_2O*, are the lowest lines of the volcano-shape plot, and therefore are responsible for the theoretical overpotential.

Physical Chemistry Chemical Physics Accepted Manuscript

The Pt_4 cluster is an outlier in the plot in Figure 8(a), due to the exceptionally large CO adsorption energy, and was considered as an individual case (not fitted with the other four metal clusters). For the other clusters, Ni is shown to be the closest to the top of the "volcano", followed by Co and Fe. Cu showed the largest overpotential among the four clusters. In Figure 8(b), $OH^* \rightarrow * + H_2O$ and $CH_3O^* \rightarrow O^* + CH_4$ are the lowest lines of the volcano plot. Four metal clusters, Fe_4, Co_4, Ni_4 and Cu_4, are lined up on the line of $OH^* \rightarrow * + H_2O$, while Pt_4 landed on the line of $CH_3O^* \rightarrow O^* + CH_4$. The approximate overpotentials are in the order $Cu_4 < Pt_4 < Co_4 < Fe_4 < Ni_4$. Combining the information from both Figures 8(a) and (b), the total overpotential of each metal is the largest calculated overpotential in either figure, and it is in the order $Co_4 < Fe_4 < Ni_4 < Cu_4 < Pt_4$, which indicates the ordering of the cluster reactivities.

Possible side reactions and cluster deactivations are not included in the plots in this analysis of the overpotentials and they may affect the conclusions. Although Fe_4, Co_4 and Ni_4 clusters showed smaller overpotentials than Cu_4 and Pt_4, the reaction pathway induced by spontaneous CO_2 chemisorption and C-O cleavage leading to adsorbed oxygen on the cluster may result in higher rate-limiting reaction free energies (Table 3), and could cause deactivation of the catalyst. The Pt_4 cluster showed a higher overpotential than Cu_4, due the large CO adsorption energy. The Cu_4 cluster showed an intermediate theoretical overpotential among the five metal clusters without any significant side reactions in this study. The Cu cluster results suggest that metal alloy clusters composed of Co and Cu, for example, may be very favorable for the electrochemical reduction of CO_2 to CH_4, possibly providing higher reactivity than a Cu cluster itself, while reducing the possibility of side reactions found for Co clusters.

3. *Competing Reactions with CH_4 Production*

In addition to the production of CH_4 from CO_2, there are other competing reactions. Figure 9 shows some competing reaction pathways that produce H_2, CO and HCOOH. Figure 9(a) shows the reaction pathways for the hydrogen evolution reaction (HER) on the five clusters (Fe_4, Co_4, Ni_4, Cu_4 and Pt_4) and the limiting potentials required for this reaction. The Cu_4 cluster shows the smallest limiting potential among the five clusters, and Fe showed a slightly higher limiting potential, followed by Co and Pt. Ni showed the highest limiting potential for HER.

The electrochemical pathway for producing CH_4 can also generate CO and HCOOH as shown in Figures 9(b) and 9(c), respectively. The release of CO follows the formation of CO*,

Physical Chemistry Chemical Physics Accepted Manuscript

and HCOOH is produced from the hydrogenation of COOH*. For CO production, the CO dissociation from the cluster corresponds to the rate-limiting step, thus CO binding energies determine the rate-limiting reaction free energies. The Cu_4 cluster showed the smallest limiting potential, while Pt showed the largest, due to the CO-overbinding (Section 2.3). The formation of HCOOH follows a different trend as a function of metal; the Cu_4 cluster showed the largest limiting potential for the reaction. The reactions of Co systems are thermodynamically favorable and require no external potential. Generally speaking, the limiting potentials of producing fuels from the electrochemical reduction of CO_2 using the five metal clusters are in the order HCOOH < CH_4 < CO.

4. Electrochemical Reduction of CO_2 on Graphene Supported Cu_4 Cluster

In order to directly compare with previous computational studies of graphene supported Cu nanoparticles and surfaces, graphene supported Cu_4 cluster was studied and the calculations were carried out using GGA_PBE method with a plane wave basis set in VASP package. The results for defective graphene supported Cu_4 (denoted as Cu_4/def-graphene) are given in Figure 10. The Cu_4 cluster supported on a defect site (a missing carbon atom) on graphene was found to have better catalytic properties than either the Cu_4 cluster and Cu_4/graphene, with a smaller limiting potential for producing CH_4 (-1.13 V, -1.27 V and -0.96 V for Cu_4, Cu_4/graphene and Cu_4/def-graphene, respectively, Figure 10). It also has a much larger limiting potential for hydrogen evolution reaction (-0.77 V). It is worth noting that, for CH_4 production, the rate-limiting step for both the Cu_4 cluster and Cu_4/graphene systems is CO* → CHO*, while that of Cu_4/def-graphene becomes the last step, OH* → * + H_2O (Figure 10). In addition, the limiting potentials of producing CO and HCOOH using Cu_4/def-graphene are calculated to be -1.26 and -0.72 V, respectively, which are much larger than those using Cu_4 cluster (-0.67 V for CO production and -0.50 V for HCOOH production). This indicates that the reactions competing with CH_4 are less favorable on Cu_4/def-graphene than those on the isolated Cu_4 cluster, suggesting a better selectivity of CH_4 on Cu_4/def-graphene, relative to the competing products, H_2, CO and HCOOH.

As discussed in Section 2.3, the two elementary steps, CO* → CHO* and OH* → * + H_2O, are the key steps of producing CH_4. Therefore, these two steps were compared among Cu_4, Cu_4/graphene and Cu_4/def-graphene from this work, as well as with the previously reported

Physical Chemistry Chemical Physics Accepted Manuscript

results for a Cu(111) surface[26], a Cu(211) surface[17], a Cu_{55} nanoparticle and a Cu_{55} nanoparticle on defected graphene[26]. In order to make a direct comparison of these systems, the PBE method and a temperature of 18.5°C were utilized to match previous calculations. Table 3 shows the calculated reaction energies for the CO* → CHO* and OH* → * + H_2O steps and for producing H_2, using the different Cu materials by the present work and the previous studies.

To begin with, the temperature change from 18.5 to 25 °C showed no significant effect on the reaction free energy for Cu_4 systems. (Table 3). Also the B3LYP functional generally showed good agreement with PBE functional (the reaction energies are only different by < 0.18 eV). Based on the PBE results, for the CO* → CHO* step, Cu_4/graphene showed a 0.14 eV higher reaction free energy than Cu_4, while the Cu_4/def-graphene showed an extremely low free energy for this step (0.11 eV). However, a different effect was obtained for the OH* → * + H_2O step; compared to Cu_4, Cu_4/graphene decreased the reaction free energy of this step to -0.02 eV, while Cu_4/def-graphene increased it to 0.96 eV. It is worth noting that the effect of the defective graphene on the CO* → CHO* step is much greater than that of the regular graphene support, suggesting a much stronger interaction between Cu_4 and the defective graphene support. This strong interaction is induced by the atomic vacancy of the graphene sheet, allowing more bonding and shared electron density between Cu_4 and graphene. A Bader charge analysis was carried out and showed that the charges on the Cu_4 clusters of Cu_4/graphene and Cu_4/def-graphene are +0.08 and +0.73, respectively (Details of partial charges see Section S4, Supporting Information). This indicates a charge transfer from the Cu_4 to the graphene support occurs, and the defective graphene gained much more charge from Cu_4 than the regular graphene. This causes the Cu d orbitals of Cu_4/def-graphene to be more vacant and available to the adsorbates, similar to the metal clusters, Fe_4, Co_4 and Ni_4. Therefore, the strong support effect by the defective graphene leads to a switch of the rate-limiting step from CO* → CHO* to OH* → * + H_2O for Cu_4/defective graphene (OH* → * + H_2O is the rate-limiting step for Fe_4, Co_4 and Ni_4).

For the previously reported Cu materials (Cu_{55}, Cu (111) and Cu(211)) listed in Table 3, CO* → CHO* was calculated to be the rate-limiting step, similar to what we find with Cu_4 and Cu_4/graphene. The defective graphene support reduced the reaction free energy of the CO* → CHO* step for Cu_{55} clusters (by 0.15 eV), and reduced that for the Cu_4 cluster (by 1.02eV), indicating that the support effect for Cu_4 tends to be much greater than for Cu_{55}. Comparing the Cu_4 system with previously reported Cu_{55} and Cu surfaces, Cu_4 shows a comparable limiting step

Physical Chemistry Chemical Physics Accepted Manuscript

free energy (0.96 eV) with that of Cu(111) surface (0.97 eV), while the Cu_{55} particle and Cu(211) surface both showed somewhat lower rate-limiting step free energies.

Besides the rate-limiting step that determines the overpotential required for producing CH_4, the hydrogen evolution reaction (HER) is another important reaction for the electrochemical reduction of CO_2. Because HER is competitive with CO_2 reduction, a catalyst that promotes CO_2 reduction while preventing HER is desirable. As shown in Table 3, all the previously reported Cu materials tend to give very low limiting free energies for the HER reaction, suggesting a high rate of formation of H_2. In the present work, Cu_4 and Cu_4/graphene also both give low limiting free energies of HER; however, Cu_4/def-graphene gave a much higher limiting free energy (0.77 eV), indicating a much lower reaction rate of HER. In addition, Cu_4/def-graphene also showed a larger limiting potential of producing CO (-1.26 V) than that of producing CH_4 (-0.96V), while for the other Cu_4 systems and previously reported Cu materials, production of CO showed a much smaller limiting potential than that of CH_4. This implies that Cu_4/def-graphene improves the selectivity of producing CH_4.

Compared to previously reported materials, although Cu_4 systems did not show a significant advantage for the limiting potential of CH_4 formation, the HER has a much higher limiting potential on Cu_4/def-graphene. The CO production on Cu_4/def-graphene also showed a higher limiting potential than CH_4. It is clear from these results that the cluster support can have a large effect on the reaction free energies of Cu_4 systems. In the case of electrochemical reduction of CO_2 to CH_4, the defective graphene supported Cu_4 showed an extremely low reaction free energy for the CO* → CHO* step (0.11 eV), which is the limiting step for all the other studied Cu_4 materials, while the rate-limiting step of the Cu_4/def-graphene switched to the OH* → * + H_2O step (0.96 eV). This is due to the strong electronic interaction between the support and the cluster.

Conclusions

Computational studies of electrochemical reduction of CO_2 to CO, HCOOH and CH_4 were carried out on five tetra-atomic transition metal clusters, Fe_4, Co_4, Ni_4, Cu_4 and Pt_4. Reaction mechanisms and thermodynamics were investigated at the B3LYP level of theory. The following conclusions are drawn from this study.

Physical Chemistry Chemical Physics Accepted Manuscript

1. The calculated overpotentials of producing CH_4 are in the order: $Co_4 < Fe_4 < Ni_4 < Cu_4 < Pt_4$ with both Co_4 and Fe_4 having overpotentials less than 1 V, indicating that small clusters can act as electrochemical catalysts for CO_2 reduction.
2. Volcano plots were derived to describe the theoretical overpotentials of electrochemical reduction of CO_2 to CH_4. Two elementary steps, CO* → CHO* and OH* → * + H_2O, were found to be the key reaction steps of determining the overpotentials for producing CH_4 for the tetra-atomic clusters and could be used to optimize metal cluster performance through size and composition variation.
3. Investigation of the possible effect of a support was carried out for the Cu_4 cluster. Calculations were done with a Cu_4 cluster on both graphene and on a graphene defect site (single atom vacancy). The latter was found to have a smaller limiting potential for producing CH_4 comparable to that of a Cu (111) surface. However, the strong interaction of the defective graphene support with the Cu_4 cluster has the advantage that it significantly increases the limiting potentials for the reactions competing with CH_4, such as the hydrogen evolution reaction (HER), and CO production.

The results suggest that small metal clusters have much potential for CO_2 reduction because their catalytic properties could be optimized based on size, metal composition and various support materials. For instance, metal alloy clusters composed of Co and Cu, may provide better reactivity than Cu clusters while reducing the possibility of side reactions from Co clusters.

Acknowledgement

This work was supported by the U.S. Department of Energy under Contract DE-AC0206CH11357 from Division of Materials Science and Engineering, Basic Energy Sciences, Office of Science. We gratefully acknowledge the computing resources provided on "Fusion", a 320-node computing cluster operated by the Laboratory Computing Resource Center at Argonne National Laboratory (ANL). We also thank the support of the Director's Postdoctoral Fellowship from ANL.

References

1. G. Centi and S. Perathoner, *Top. Catal.*, 2009, 52, 948-961.
2. E. V. Kondratenko, G. Mul, J. Baltrusaitis, G. O. Larrazábal and J. Pérez-Ramírez, *Energy Environ. Sci.*, 2013, 6, 3112.
3. M. Cokoja, C. Bruckmeier, B. Rieger, W. A. Herrmann and F. E. Kühn, *Angew. Chem., Int. Ed.*, 2011, 50, 8510-8537.
4. D. Cheng, F. R. Negreiros, E. Aprà and A. Fortunelli, *ChemSusChem*, 2013, 6, 944-965.
5. M. Gattrell, N. Gupta and A. Co, *J. Electroanal. Chem.*, 2006, 594, 1-19.

Physical Chemistry Chemical Physics Accepted Manuscript

6. M. Gangeri, S. Perathoner, S. Caudo, G. Centi, J. Amadou, D. Bégin, C. Pham-Huu, M. J. Ledoux, J. P. Tessonnier, D. S. Su and R. Schlögl, *Catal. Today*, 2009, 143, 57-63.
7. Y. Hori, I. Takahashi, O. Koga and N. Hoshi, *J. Mol. Catal. A: Chem.*, 2003, 199, 39-47.
8. N. S. Spinner, J. A. Vega and W. E. Mustain, *Catal. Sci. Technol.*, 2012, 2, 19.
9. G. Centi, S. Perathoner, G. Win and M. Gangeri, *Green Chem.*, 2007, 9, 671.
10. D. T. Whipple and P. J. A. Kenis, *J. Phys. Chem. Lett*, 2010, 1, 3451-3458.
11. G. Centi and S. Perathoner, *ChemSusChem*, 2010, 3, 195-208.
12. B. Kumar, M. Llorente, J. Froehlich, T. Dang, A. Sathrum and C. P. Kubiak, *Annu. Rev. Phys. Chem.*, 2012, 63, 541-569.
13. E. E. Benson, C. P. Kubiak, A. J. Sathrum and J. M. Smieja, *Chem. Soc. Rev.*, 2009, 38, 89.
14. K. P. Kuhl, E. R. Cave, D. N. Abram and T. F. Jaramillo, *Energy Environ. Sci.*, 2012, 5, 7050.
15. Y. Hori, in *Modern Aspects of Electrochemistry*, eds. C. Vayenas, R. White and M. Gamboa-Aldeco, Springer New York, 2008, vol. 42, ch. 3, pp. 89-189.
16. K. J. P. Schouten, Y. Kwon, C. J. M. van der Ham, Z. Qin and M. T. M. Koper, *Chem. Sci.*, 2011, 2, 1902.
17. A. A. Peterson, F. Abild-Pedersen, F. Studt, J. Rossmeisl and J. K. Nørskov, *Energy Environ. Sci.*, 2010, 3, 1311.
18. Y. Hori, H. Wakebe, T. Tsukamoto and O. Koga, *Surf. Sci.*, 1995, 335, 258-263.
19. F. Calle-Vallejo and M. T. M. Koper, *Angew. Chem., Int. Ed.*, 2013, 52, 7282-7285.
20. B. Z. Nikolic, H. Huang, D. Gervasio, A. Lin, C. Fierro, R. R. Adzic and E. Yeager, *J. Electroanal. Chem. Interfacial Electrochem.*, 1990, 295, 415-423.
21. N. Hoshi, T. Uchida, T. Mizumura and Y. Hori, *J. Electroanal. Chem.*, 1995, 381, 261-264.
22. N. Hoshi, H. Ito, T. Suzuki and Y. Hori, *J. Electroanal. Chem.*, 1995, 395, 309-312.
23. J. Bugayong and G. L. Griffin, *ECS Trans.*, 2013, 58, 81-89.
24. Y. Koo, R. Malik, N. Alvarez, L. White, V. N. Shanov, M. Schulz, B. Collins, J. Sankar and Y. Yun, *RSC Adv.*, 2014, 4, 16362.
25. Y. Chen, C. W. Li and M. W. Kanan, *J. Am. Chem. Soc.*, 2012, 134, 19969-19972.
26. D.-H. Lim, J. H. Jo, D. Y. Shin, J. Wilcox, H. C. Ham and S. W. Nam, *Nanoscale*, 2014.
27. P. Hirunsit, *J. Phys. Chem. C*, 2013, 117, 8262-8268.
28. R. Reske, M. Duca, M. Oezaslan, K. J. P. Schouten, M. T. M. Koper and P. Strasser, *J. Phys. Chem. Lett*, 2013, 4, 2410-2413.
29. C. W. Li and M. W. Kanan, *J. Am. Chem. Soc.*, 2012, 134, 7231-7234.
30. K. Okamoto, R. Akiyama, H. Yoshida, T. Yoshida and S. Kobayashi, *J. Am. Chem. Soc.*, 2005, 127, 2125-2135.
31. S. Lee, B. Lee, F. Mehmood, S. Seifert, J. A. Libera, J. W. Elam, J. Greeley, P. Zapol, L. A. Curtiss, M. J. Pellin, P. C. Stair, R. E. Winans and S. Vajda, *J. Phys. Chem. C*, 2010, 114, 10342-10348.
32. L. M. Molina, S. Lee, K. Sell, G. Barcaro, A. Fortunelli, B. Lee, S. Seifert, R. E. Winans, J. W. Elam and M. J. Pellin, *Catal. Today*, 2011, 160, 116-130.
33. F. R. Negreiros, L. Sementa, G. Barcaro, S. Vajda, E. Aprá and A. Fortunelli, *ACS Catal.*, 2012, 2, 1860-1864.
34. E. C. Tyo, C. Yin, M. Di Vece, Q. Qian, G. Kwon, S. Lee, B. Lee, J. E. DeBartolo, S. Seifert, R. E. Winans, R. Si, B. Ricks, S. Goergen, M. Rutter, B. Zugic, M. Flytzani-Stephanopoulos, Z. W. Wang, R. E. Palmer, M. Neurock and S. Vajda, *ACS Catal.*, 2012, 2, 2409-2423.
35. G. Kwon, G. A. Ferguson, C. J. Heard, E. C. Tyo, C. Yin, J. DeBartolo, S. Seifert, R. E. Winans, A. J. Kropf, J. Greeley, R. L. Johnston, L. A. Curtiss, M. J. Pellin and S. Vajda, *ACS Nano*, 2013, 7, 5808-5817.
36. Y. Gao, N. Shao, Y. Pei, Z. Chen and X. C. Zeng, *ACS Nano*, 2011, 5, 7818-7829.
37. G. A. Ferguson, F. Mehmood, R. B. Rankin, J. P. Greeley, S. Vajda and L. A. Curtiss, *Top. Catal.*, 2012, 55, 353-365.
38. F. Mehmood, J. Greeley and L. A. Curtiss, *J. Phys. Chem. C*, 2009, 113, 21789-21796.
39. F. Mehmood, J. Greeley, P. Zapol and L. A. Curtiss, *J. Phys. Chem. B*, 2010, 114, 14458-14466.
40. S. Vajda, M. J. Pellin, J. P. Greeley, C. L. Marshall, L. A. Curtiss, G. A. Ballentine, J. W. Elam, S. Catillon-Mucherie, P. C. Redfern, F. Mehmood and P. Zapol, *Nat. Mater.*, 2009, 8, 213-216.
41. J. Russell, P. Zapol, P. Král and L. A. Curtiss, *Chem. Phys. Lett.*, 2012, 536, 9-13.
42. R. Reske, H. Mistry, F. Behafarid, B. Roldan Cuenya and P. Strasser, *J. Am. Chem. Soc.*, 2014, 140506133848009.
43. Y. Lei, F. Mehmood, S. Lee, J. Greeley, B. Lee, S. Seifert, R. E. Winans, J. W. Elam, R. J. Meyer, P. C. Redfern, D. Teschner, R. Schlogl, M. J. Pellin, L. A. Curtiss and S. Vajda, *Science*, 2010, 328, 224-228.
44. S. Proch, M. Wirth, H. S. White and S. L. Anderson, *J. Am. Chem. Soc.*, 2013, 135, 3073-3086.
45. D. R. Kauffman, D. Alfonso, C. Matranga, H. Qian and R. Jin, *J. Am. Chem. Soc.*, 2012, 134, 10237-10243.
46. C. Liu, T. R. Cundari and A. K. Wilson, *Inorg. Chem.*, 2011, 50, 8782-8789.
47. C. Liu, T. R. Cundari and A. K. Wilson, in *Applications of Molecular Modeling to Challenges in Clean Energy*, American Chemical Society, 2013, vol. 1133, ch. 5, pp. 67-88.
48. C. Liu, L. Munjanja, T. R. Cundari and A. K. Wilson, *J. Phys. Chem. A*, 2010, 114, 6207-6216.
49. C. Liu, T. R. Cundari and A. K. Wilson, *J. Phys. Chem. C*, 2012, 116, 5681-5688.
50. I. A. Shkrob, T. W. Marin, H. He and P. Zapol, *J. Phys. Chem. C*, 2012, 116, 9450-9460.
51. N. M. Dimitrijevic, B. K. Vijayan, O. G. Poluektov, T. Rajh, K. A. Gray, H. He and P. Zapol, *J. Am. Chem. Soc.*, 2011, 133, 3964-3971.
52. H. He, P. Zapol and L. A. Curtiss, *Energy Environ. Sci.*, 2012, 5, 6196.
53. H. He, P. Zapol and L. A. Curtiss, *J. Phys. Chem. C*, 2010, 114, 21474-21481.
54. A. D. Becke, *J. Chem. Phys.*, 1993, 98, 5648.
55. C. Lee, W. Yang and R. G. Parr, *Phys. Rev. B*, 1988, 37, 785-789.
56. M. J. Frisch, 2009.
57. Y. Zhao and D. G. Truhlar, *Theor. Chem. Acc.*, 2007, 120, 215-241.
58. J. P. Perdew, K. Burke and M. Ernzerhof, *Phys. Rev. Lett.*, 1996, 77, 3865-3868.
59. J. P. Perdew, K. Burke and M. Ernzerhof, *Phys. Rev. Lett.*, 1997, 78, 1396-1396.
60. C. Adamo and V. Barone, *J. Chem. Phys.*, 1999, 110, 6158.
61. G. D. Purvis, *J. Chem. Phys.*, 1982, 76, 1910.
62. A. V. Mitin, J. Baker and P. Pulay, *J. Chem. Phys.*, 2003, 118, 7775.
63. P. J. Hay and W. R. Wadt, *J. Chem. Phys.*, 1985, 82, 270.

Physical Chemistry Chemical Physics Accepted Manuscript

64. P. J. Hay and W. R. Wadt, *J. Chem. Phys.*, 1985, 82, 299.
65. W. R. Wadt and P. J. Hay, *J. Chem. Phys.*, 1985, 82, 284.
66. J. P. Foster and F. Weinhold, *J. Am. Chem. Soc.*, 1980, 102, 7211-7218.
67. A. E. Reed and F. Weinhold, *J. Chem. Phys.*, 1983, 78, 4066-4073.
68. A. E. Reed, R. B. Weinstock and F. Weinhold, *J. Chem. Phys.*, 1985, 83, 735.
69. A. E. Reed and F. Weinhold, *J. Chem. Phys.*, 1985, 83, 1736.
70. A. E. Reed, L. A. Curtiss and F. Weinhold, *Chem. Rev.*, 1988, 88, 899-926.
71. J. E. Carpenter and F. Weinhold, *J. Mol. Struct.: THEOCHEM*, 1988, 169, 41-62.
72. J. K. Nørskov, J. Rossmeisl, A. Logadottir, L. Lindqvist, J. R. Kitchin, T. Bligaard and H. Jónsson, *J. Phys. Chem. B*, 2004, 108, 17886-17892.
73. A. A. Peterson and J. K. Nørskov, *J. Phys. Chem. Lett*, 2012, 3, 251-258.
74. M. J. Janik, C. D. Taylor and M. Neurock, *J. Electrochem. Soc.*, 2009, 156, B126.
75. V. Tripković, E. Skúlason, S. Siahrostami, J. K. Nørskov and J. Rossmeisl, *Electrochim. Acta*, 2010, 55, 7975-7981.
76. G. Kresse, *Phys. Rev. B: Condens. Matter*, 1993, 47, 558-561.
77. G. Kresse, *Phys. Rev. B: Condens. Matter*, 1994, 49, 14251-14269.
78. G. Kresse, *Phys. Rev. B: Condens. Matter*, 1996, 54, 11169-11186.
79. G. Kresse, *Comput. Mater. Sci*, 1996, 6, 15-50.
80. W. Wang, D. Zheng, C. Du, Z. Zou, X. Zhang, B. Xia, H. Yang and D. L. Akins, *J. Power Sources*, 2007, 167, 243-249.
81. M. H. Khedr, A. A. Omar and S. A. Abdel-Moaty, *Mater. Sci. Eng., A*, 2006, 432, 26-33.
82. C.-T. Hsieh and J.-Y. Lin, *J. Power Sources*, 2009, 188, 347-352.
83. Y. Yourdshahyan, V. R. Cooper, A. M. Kolpak and A. M. Rappe, *Proc. SPIE 5223, Physical Chemistry of Interfaces and Nanomaterials II*, 2003, 223-231.

Physical Chemistry Chemical Physics Accepted Manuscript

Tables and Figures

Table of Content:

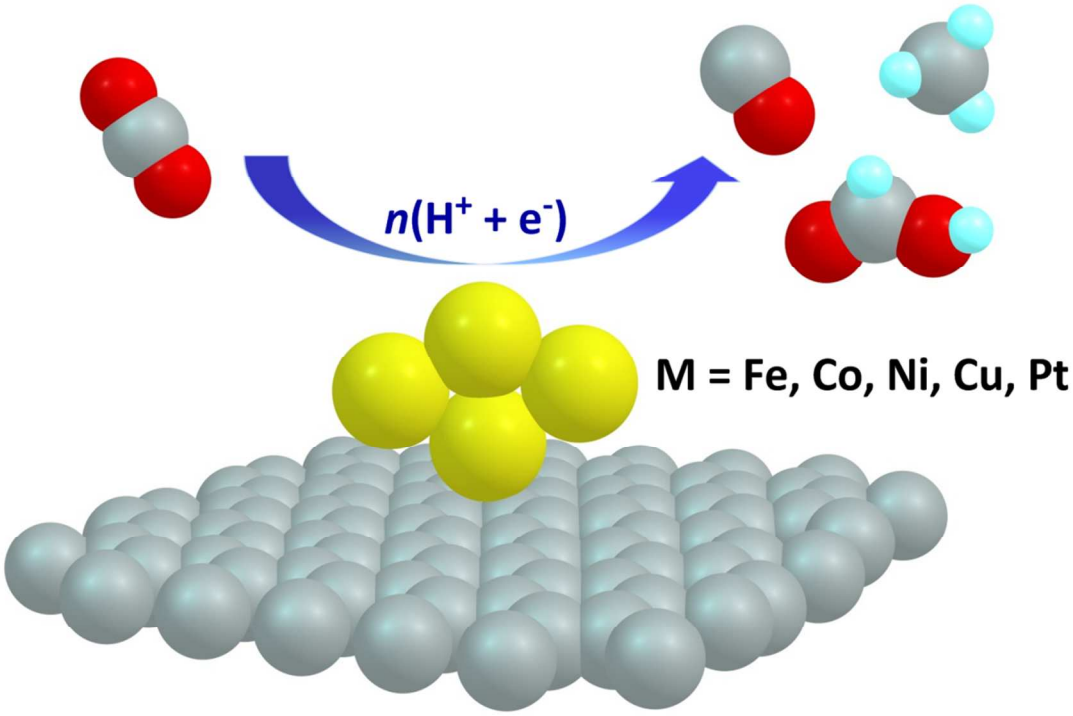

Computational studies of electrochemical reduction of CO_2 were carried out using tetra-atomic transition metal clusters.

Physical Chemistry Chemical Physics Accepted Manuscript

Table 1. Structural, electronic and thermodynamic data of chemisorption and electrochemical adsorption of CO_2 on tetra-atomic clusters

Metal Clusters		Chemisorption			Electrochemical Adsorption	
		CO_2*	Partial Charge on CO_2 Moiety (e)	Adsorption Free Energies (eV)	COOH*	Reaction Free Energies (eV)
Fe_4		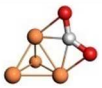	-0.67	-0.55	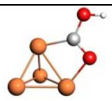	0.01
Co_4		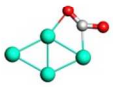	-0.64	-0.37		-0.08
Ni_4		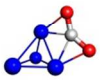	-0.52	-0.87	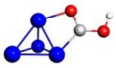	-0.67
Cu_4		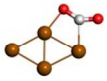	-0.38	0.27	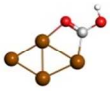	0.50
Rh_4			-0.35	0.14		0.52
Pd_4			0.04	0.28		0.80
Ag_4			0.05	0.31		1.40
Ir_4			0.01	0.38	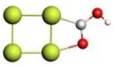	0.21
Pt_4			-0.34	0.43		0.22
Au_4			-0.4	0.28		1.43

Physical Chemistry Chemical Physics Accepted Manuscript

Table 2. The limiting reaction free energies (reaction free energies for the most endergonic step) for each cluster (OH* → H_2O + * for Fe_4, Co_4 and Ni_4, and CO* → CHO* for Cu_4 and Pt_4) and (2(OH*) → H_2O + OH*) for the side reactions of Fe_4, Co_4 and Ni_4 clusters

Cluster	Limiting Reaction Free Energies (eV)	Limiting Reaction Free Energies for Side Reaction Pathway(eV)
Fe_4	0.72	1.17
Co_4	0.63	1.04
Ni_4	1.01	1.53
Cu_4	1.05	-
Pt_4	1.32	-

Physical Chemistry Chemical Physics Accepted Manuscript

Table 3. Reaction free energies for the key steps of electrochemical reduction of CO_2 to CH_4 on different Cu materials (tw = this work)

Material	ΔG(CO* → CHO*) (eV)	ΔG(OH* → * + H_2O) (eV)	ΔG(H* → * + H_2) (eV)	Method	T (°C)	Ref.
Cu_4	1.05	0.01	0.14	B3LYP/m 6-31g*	25	tw
	1.05	0.02	0.13	B3LYP/m 6-31g*	18.5	
	1.13	0.20	0.23	PBE/PW	18.5	
Cu_4/Graphene	1.27	-0.02	0.09	PBE/PW	18.5	tw
Cu_4/Def-Graphene	0.11	0.96	0.77	PBE/PW	18.5	tw
Cu_{55}	0.83	-	-	PBE/PW	18.5	[26]
Cu_{55}/Def-Graphene	0.68	-	0.24	PBE/PW	18.5	[26]
Cu (111)	0.97	-	0.22	PBE/PW	18.5	[26]
Cu (211)	0.74	-	0.03	RPBE/PW	18.5	[17]

Physical Chemistry Chemical Physics Accepted Manuscript

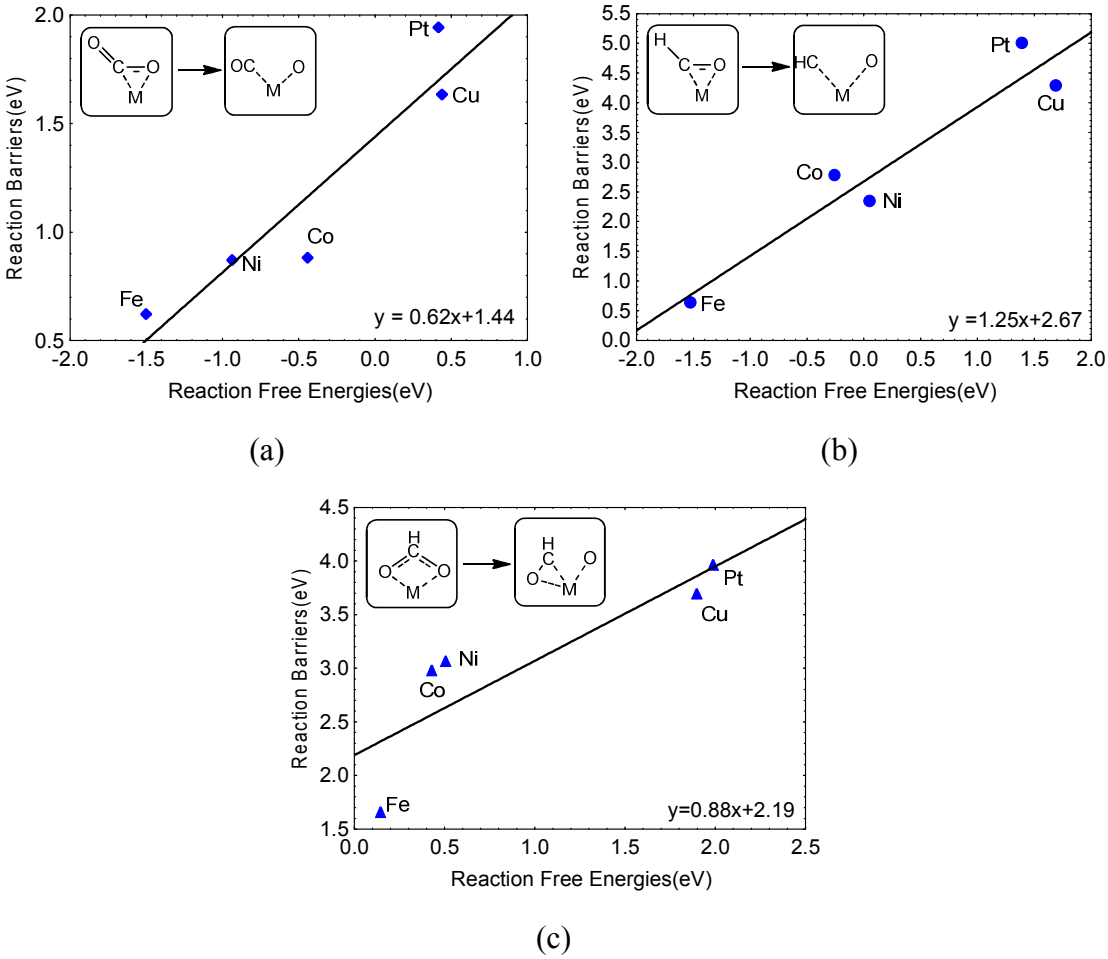

Figure 1. Brønsted–Evans–Polanyi (BEP) relations of C-O cleavage reactions of (a) CO_2* (Eq 4) (b) CHO* (Eq 5) (c) OCHO* (Eq 6)

Physical Chemistry Chemical Physics Accepted Manuscript

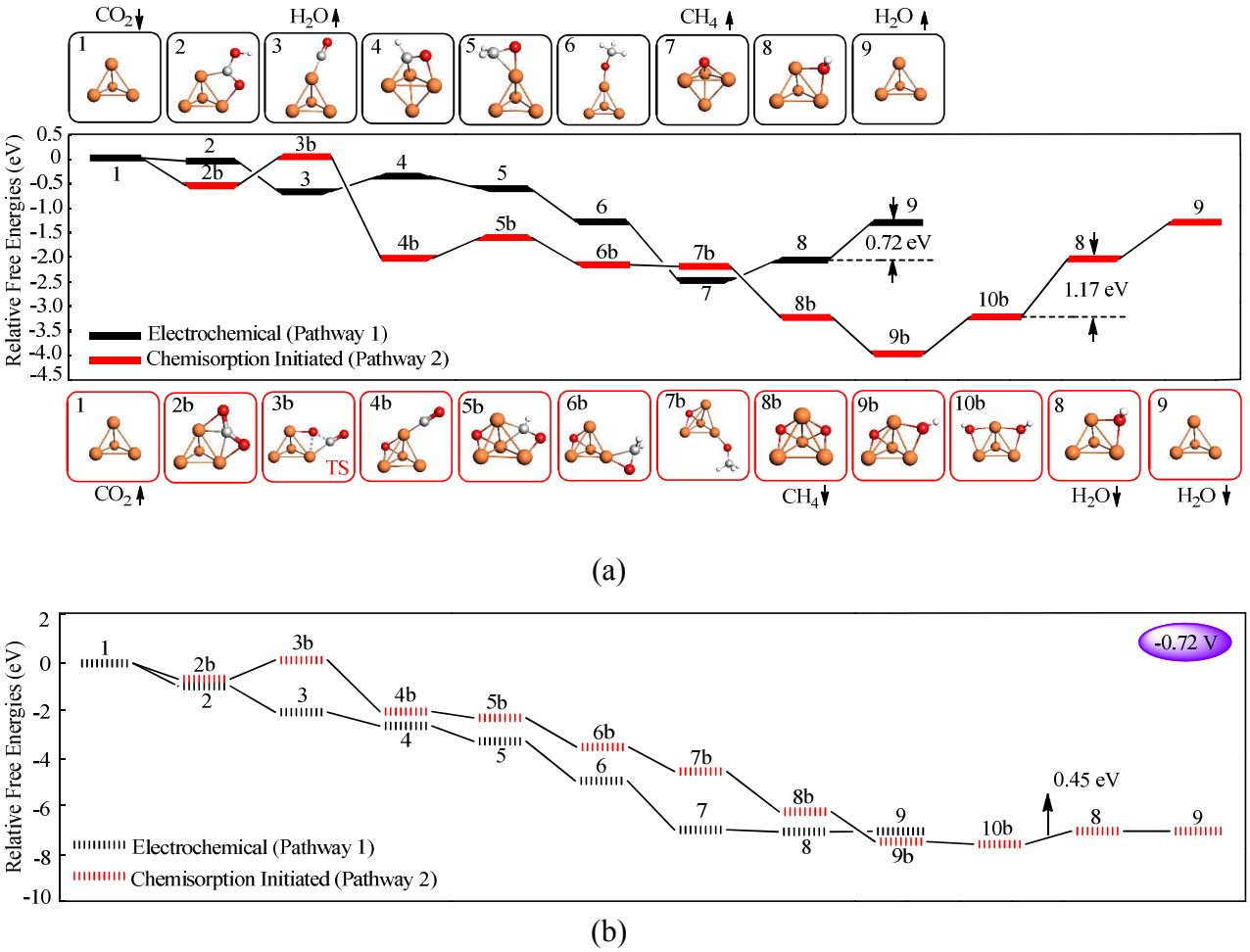

Figure 2. Reaction pathways of electrochemical reduction of CO_2 to CH_4 on a Fe_4 cluster. (a) Reaction pathways without applied potential. b) Reaction pathways at applied potential of -0.72 V. The initial state (CO_2 + *) is denoted as state **1**, and the final state (H_2O + *) is denoted as state **9**. The intermediates of pathway 1 are denoted as states **2-8**, and the intermediates and transition states of pathway 2 are denoted as states **2b-11b** and **8**. The structures on the top of figure (a) represent the states of pathway 1, and those on the bottom represent the states of pathway 2. Steps **1** → **2b**, **2b** → **3b** and **3b** → **4b** (pathway 2) are chemical reactions, while all the other steps (in both pathways) are electrochemical reactions. Each electrochemical step involves transfer of a (H^+ + e^-) pair.

Physical Chemistry Chemical Physics Accepted Manuscript

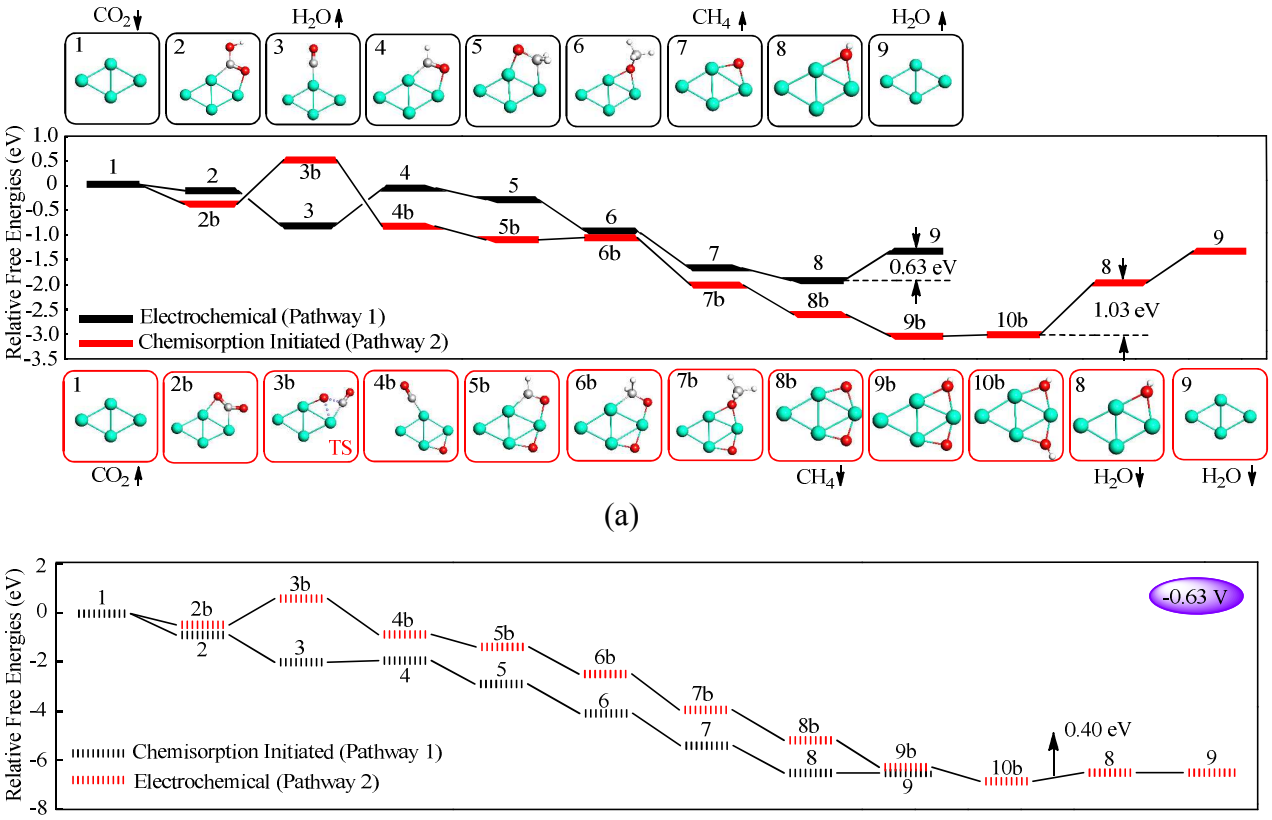

(a)

(b)

Figure 3. Reaction pathways of electrochemical reduction of CO_2 to CH_4 on a Co_4 cluster. (a) Reaction pathways without applied potential. (b) Reaction pathways at applied potential of -0.63 V. The initial state (CO_2 + *) is denoted as state **1**, and the final state (H_2O + *) is denoted as state **9**. The intermediates of pathway 1 are denoted as states **2-8**, and the intermediates and transition states of pathway 2 are denoted as states **2b-11b** and **8**. The structures on the top of figure (a) represent the states of pathway 1, and those on the bottom represent the states of pathway 2. Steps **1** → **2b**, **2b** → **3b** and **3b** → **4b** (pathway 2) are chemical reactions, while all the other steps (in both pathways) are electrochemical reactions. Each electrochemical step involves transfer of a (H^+ + e^-) pair.

Physical Chemistry Chemical Physics Accepted Manuscript

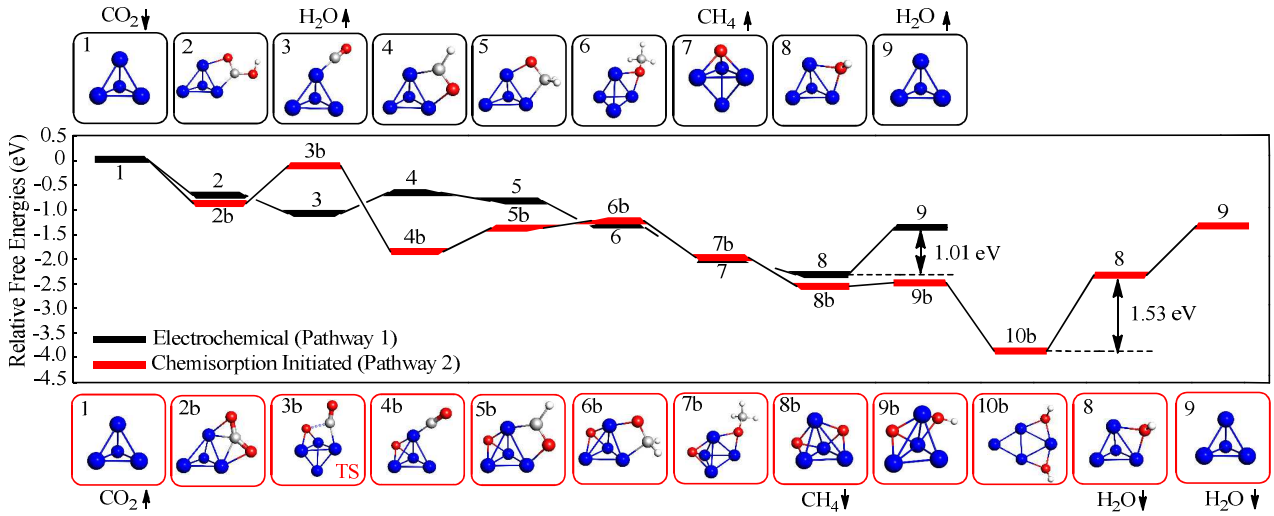

(a)

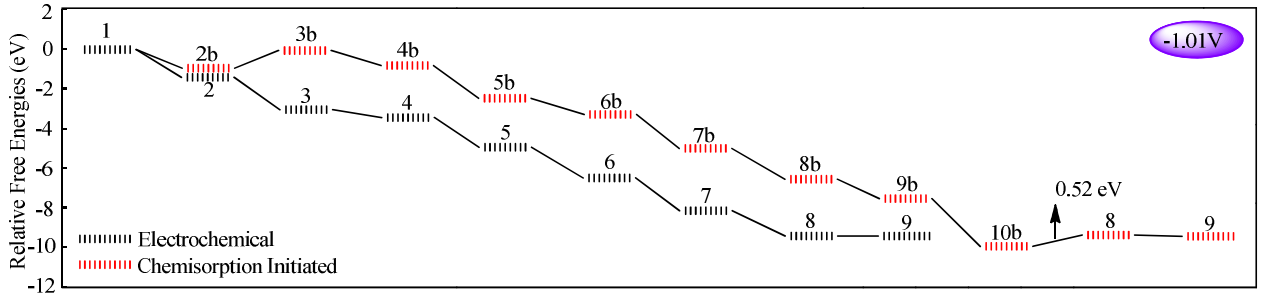

(b)

Figure 4. Reaction pathways of electrochemical reduction of CO_2 to CH_4 on a Ni_4 cluster. a) Reaction pathways without applied potential. b) Reaction pathways at applied potential of -1.01 V. The initial state (CO_2 + *) is denoted as state **1**, and the final state (H_2O + *) is denoted as state **9**. The intermediates of pathway 1 are denoted as states **2-8**, and the intermediates and transition states of pathway 2 are denoted as states **2b-11b** and **8**. The structures on the top of figure (a) represent the states of pathway 1, and those on the bottom represent the states of pathway 2. Steps **1** → **2b**, **2b** → **3b** and **3b** → **4b** (pathway 2) are chemical reactions, while all the other steps (in both pathways) are electrochemical reactions. Each electrochemical step involves transfer of a (H^+ + e^-) pair.

Physical Chemistry Chemical Physics Accepted Manuscript

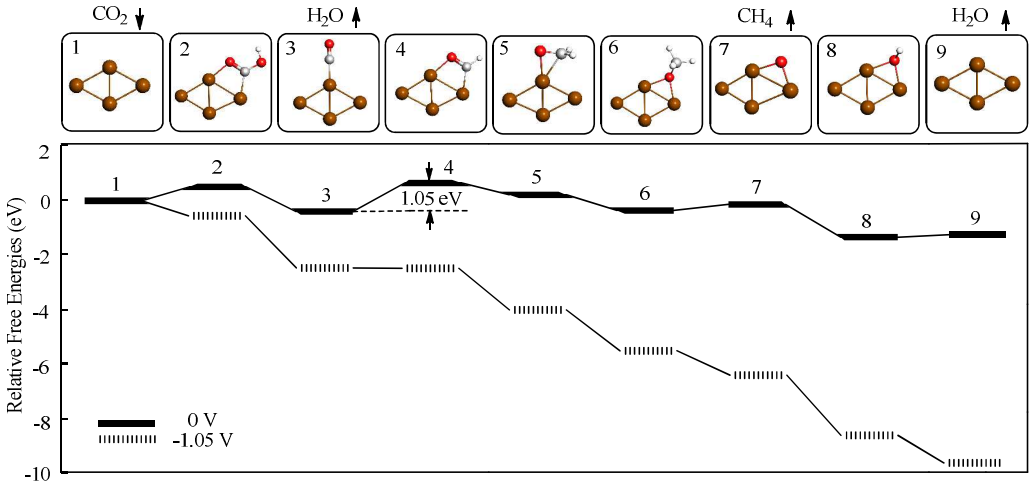

Figure 5. Reaction pathways of electrochemical reduction of CO_2 to CH_4 on a Cu_4 cluster. The solid lines represent the reaction pathways with no applied potential, and the dashed lines represent the reaction pathways at the limiting potential of -1.05 V. The initial state (CO_2 + *) is denoted as state **1**, and the final state (H_2O + *) is denoted as state **9**. The intermediates of are denoted as states **2-8**. Each elementary step involves transfer of a ($H^+ + e^-$) pair.

Physical Chemistry Chemical Physics Accepted Manuscript

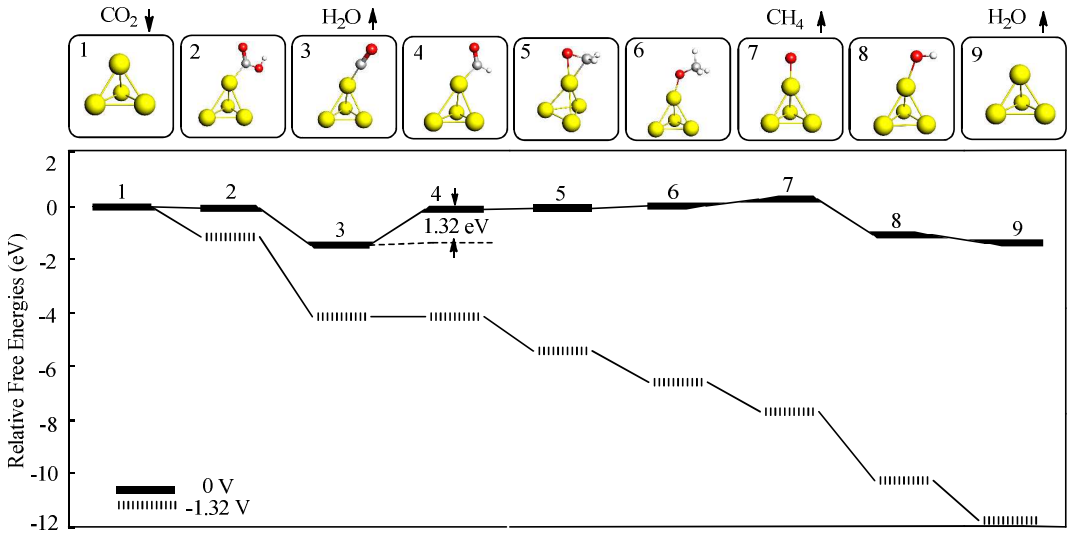

Figure 6. Reaction pathways of electrochemical reduction of CO_2 to CH_4 on a Pt_4 cluster. The solid lines represent the reaction pathways with no applied potential, and the dashed lines represent the reaction pathways at the limiting potential of -1.32V. The initial state (CO_2 + *) is denoted as state **1**, and the final state (H_2O + *) is denoted as state **9**. The intermediates of are denoted as states **2-8**. Each elementary step involves transfer of a ($H^+ + e^-$) pair.

Physical Chemistry Chemical Physics Accepted Manuscript

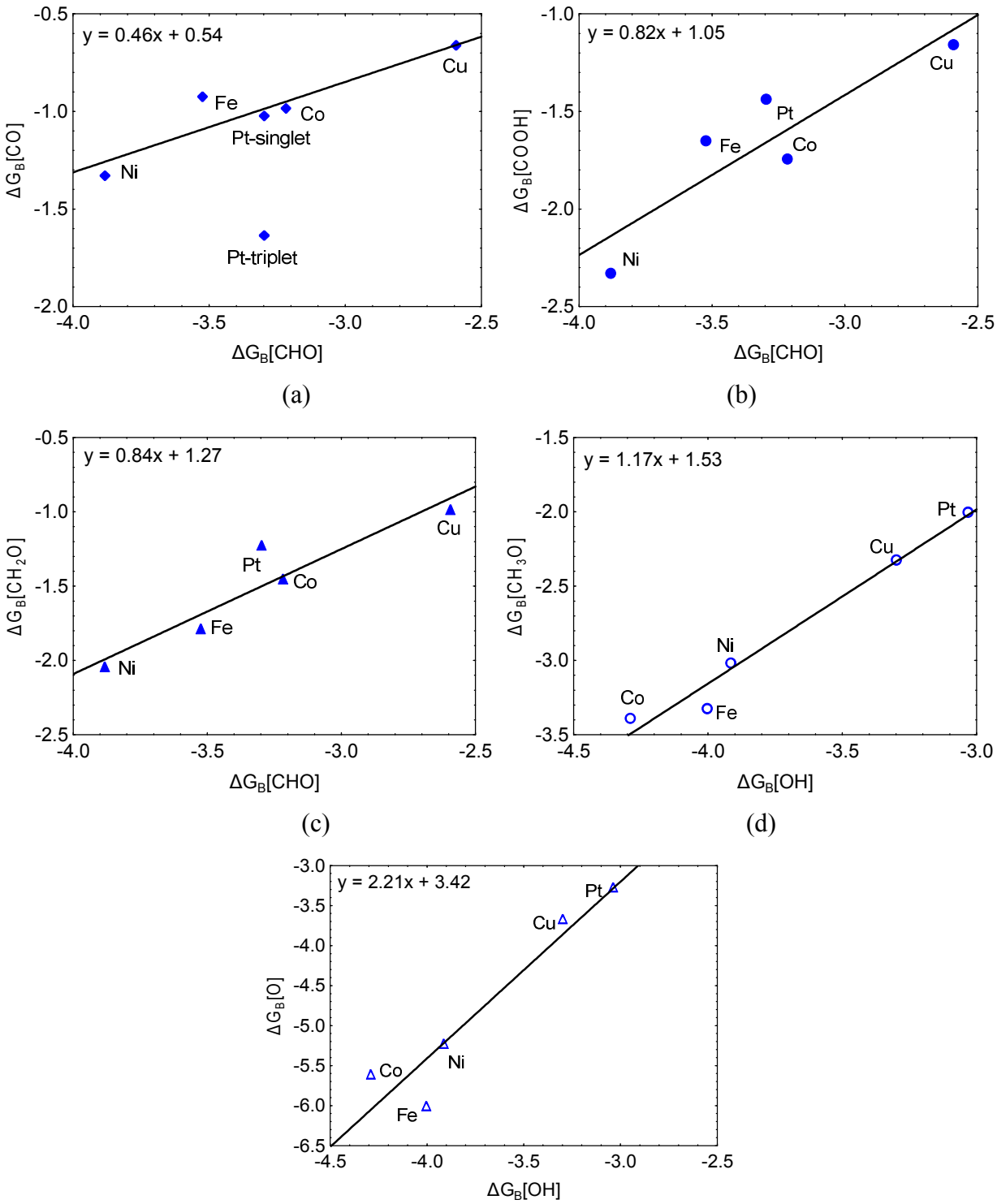

Figure 7. Adsorption free energy scaling relations of the intermediate species in the electrochemical pathway of the reduction of CO_2 to CH_4. The adsorption free energies of the carbon-bound species (CO (a), COOH (b) and CH_2O (c)) are correlated with ΔG_B[CHO], and

Physical Chemistry Chemical Physics Accepted Manuscript

those of the oxygen-bound species (CH_3O (d) and O (e)) are correlated with ΔG_B[OH]. The more negative adsorption free energies correspond to more tightly bound adsorbates. All values are in eV.

Physical Chemistry Chemical Physics Accepted Manuscript

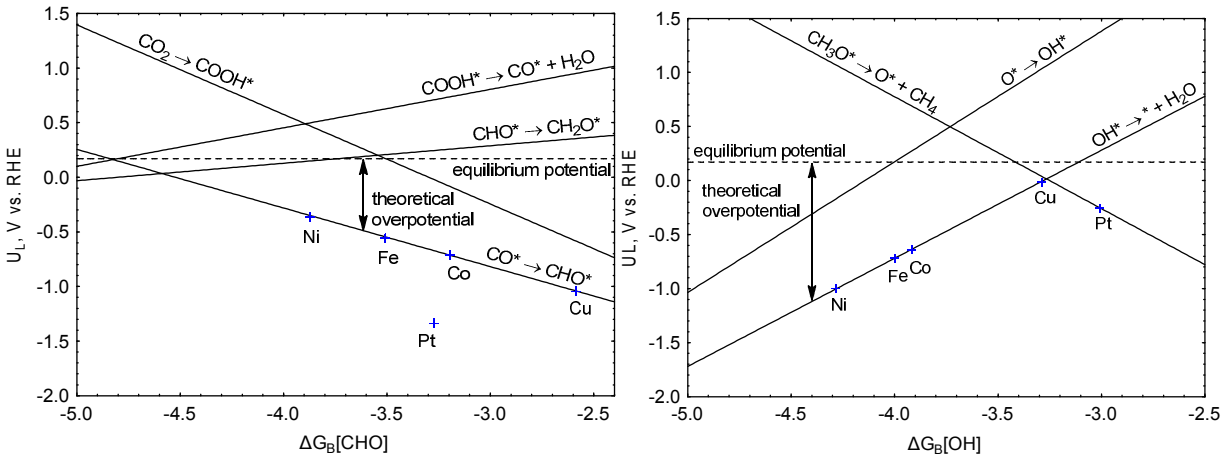

(a) (b)

Figure 8. Limiting potentials (U_L) for elementary steps of the electrochemical pathway of the reduction of CO_2 to CH_4. The dashed line represents the equilibrium potential (+0.17 V) versus RHE for the overall electrochemical reduction of CO_2 to CH_4. Each solid line is fitted by the calculated limiting potentials of the metal clusters for each elementary step. The energy difference between the equilibrium potential and U_L indicates a theoretical overpotential as a function of the considered adsorption free energies. In principle, the larger the overpotential, the more difficult for the reaction to proceed; the most negative lines in the plots correspond to the elementary steps that determine the overpotentials.

Physical Chemistry Chemical Physics Accepted Manuscript

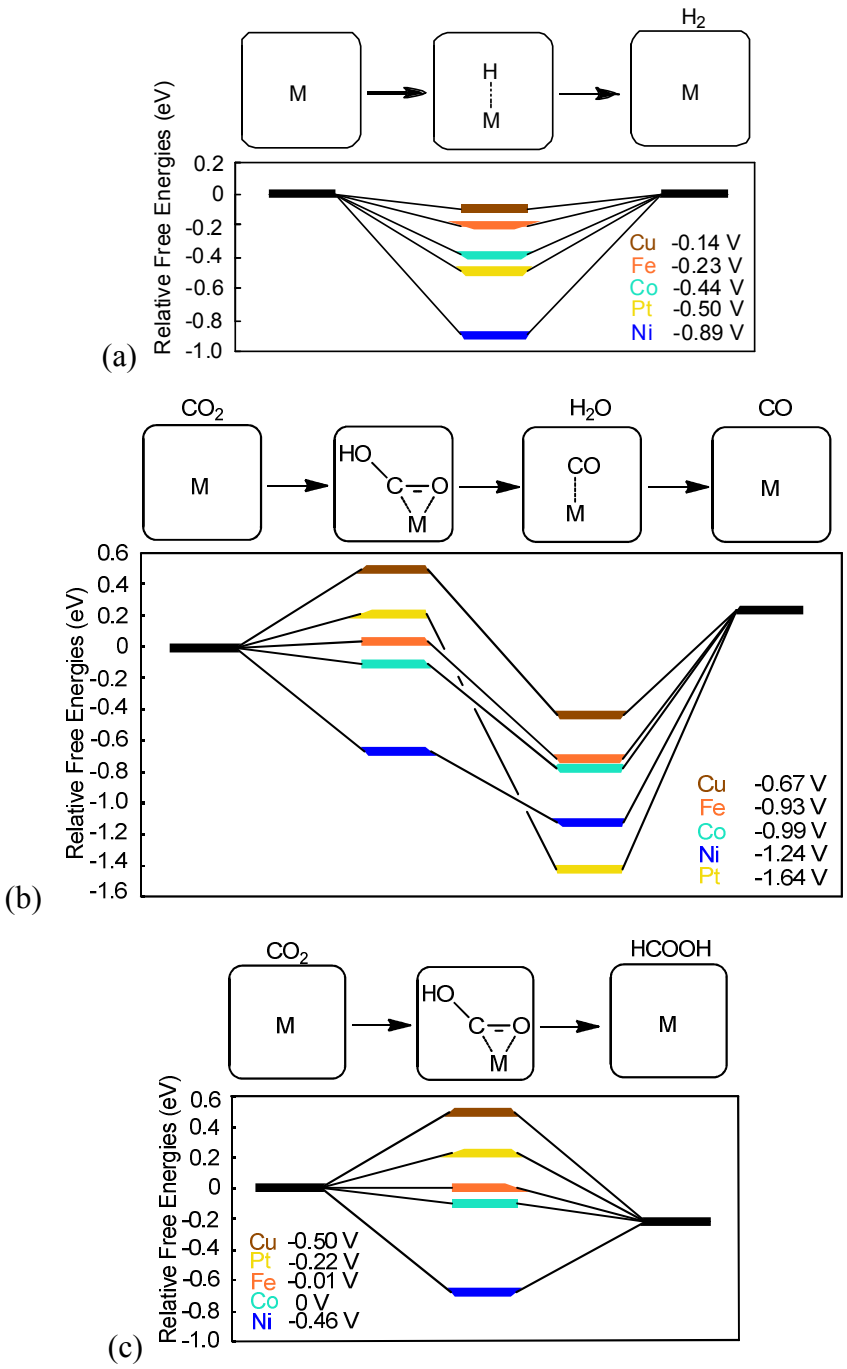

Figure 9. Reaction pathways for producing H_2 (a), CO (b) and HCOOH (c) and limiting potentials of different metal clusters. Each electrochemical step involves transfer of a ($H^+ + e^-$) pair. The numbers on the y axis represent relative free energies (eV). The limiting potentials (the potential required to proceed over the most endergonic step) of each metal cluster are listed in the legend.

Physical Chemistry Chemical Physics Accepted Manuscript

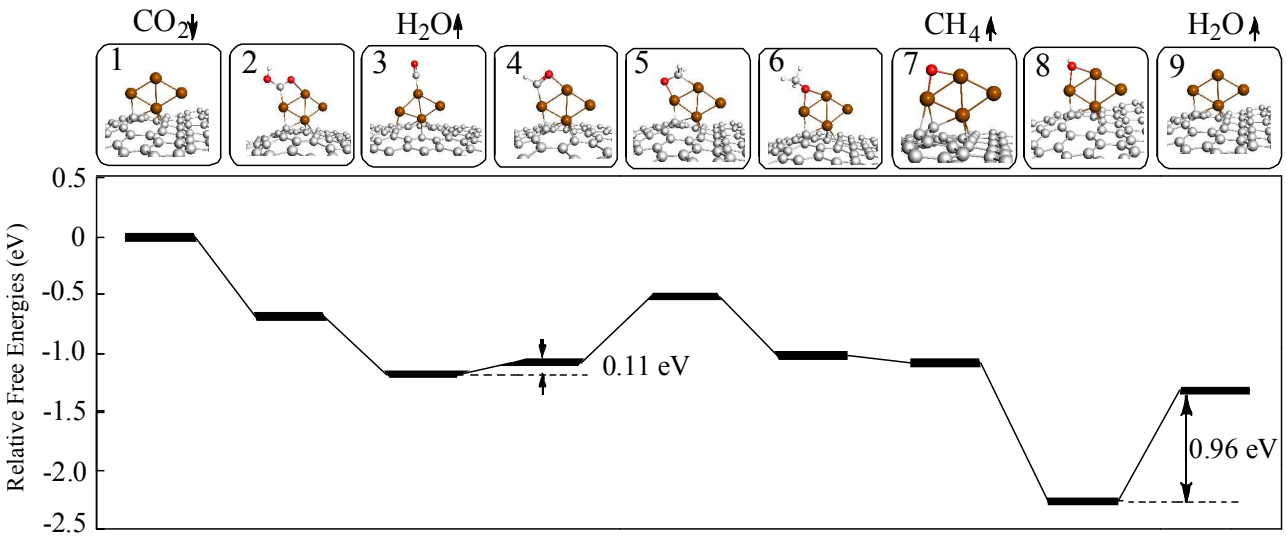

Figure 10. Reaction pathways of electrochemical reduction of CO_2 to CH_4 on defective graphene supported Cu_4 cluster. The initial state (CO_2 + *) is denoted as state **1**, and the final state (H_2O + *) is denoted as state **9**. The intermediates are denoted as states **2-8**. Each elementary step involves transfer of a (H^+ + e^-) pair.

Physical Chemistry Chemical Physics Accepted Manuscript